Received: 25 June 2024 | Revised: 11 September 2024 | Accepted: 1 October 2024

DOI: 10.1002/pld3.70017

RESEARCH ARTICLE

Broad-scale phenotyping in Arabidopsis reveals varied involvement of RNA interference across diverse plant-microbe interactions

Alessa Ruf[1] | Hannah Thieron[2] | Sabrine Nasfi[3] | Bernhard Lederer[1] | Sebastian Fricke[4] | Trusha Adeshara[5] | Johannes Postma[5] | Patrick Blumenkamp[6] | Seomun Kwon[5] | Karina Brinkrolf[6] | Michael Feldbrügge[5] | Alexander Goesmann[6] | Julia Kehr[4] | Jens Steinbrenner[3] | Ena Šečić[3] | Vera Göhre[5,7] | Arne Weiberg[1] | Karl-Heinz Kogel[3,8] | Ralph Panstruga[2] | Silke Robatzek[1] | on behalf of the exRNA consortium

[1]LMU Munich Biocenter, Planegg, Germany

[2]Unit for Plant Molecular Cell Biology, Institute for Biology I, RWTH Aachen University, Aachen, Germany

[3]Institute of Phytopathology, Centre for BioSystems, Land Use and Nutrition, Justus Liebig University, Giessen, Germany

[4]Institute of Plant Science and Microbiology, Molecular Plant Genetics, Universität, Hamburg, Germany

[5]Institute for Microbiology, Cluster of Excellence on Plant Sciences, Heinrich-Heine University Düsseldorf, Düsseldorf, Germany

[6]Bioinformatics and Systems Biology, Justus Liebig University Giessen, Germany

[7]Hochschule Darmstadt, Darmstadt, Germany

[8]Institut de biologie moléculaire des plantes, CNRS, Université de Strasbourg, Strasbourg, France

Correspondence
Silke Robatzek, LMU Munich Biocenter, Großhadener Strasse 4, 82152 Planegg, Germany.
Email: robatzek@bio.lmu.de

Abstract

RNA interference (RNAi) is a crucial mechanism in immunity against infectious microbes through the action of DICER-LIKE (DCL) and ARGONAUTE (AGO) proteins. In the case of the taxonomically diverse fungal pathogen *Botrytis cinerea* and the oomycete *Hyaloperonospora arabidopsidis*, plant DCL and AGO proteins have proven roles as negative regulators of immunity, suggesting functional specialization of these proteins. To address this aspect in a broader taxonomic context, we characterized the colonization pattern of an informative set of *DCL* and *AGO* loss-of-function mutants in *Arabidopsis thaliana* upon infection with a panel of pathogenic microbes with different lifestyles, and a fungal mutualist. Our results revealed that, depending on the interacting pathogen, AGO1 acts as a positive or negative regulator of immunity, while AGO4 functions as a positive regulator. Additionally, AGO2 and AGO10 positively modulated the colonization by a fungal mutualist. Therefore, analyzing the role of RNAi across a broader range of plant-microbe interactions has identified previously unknown functions for AGO proteins. For some pathogen interactions, however, all tested mutants exhibited wild-type-like infection phenotypes, suggesting that the roles of AGO and DCL proteins in these interactions may be more complex to elucidate.

Alessa Ruf, Hannah Thieron, and Sabrine Nasfi contributed equally to the study.

Funding information
Deutsche Forschungsgemeinschaft (DFG), Grant/Award Numbers: FE448/15-1, GO 2037/8-1, GO 2064/4-1, KE 856/8-1, KO 1208/32-1, PA 861/22-1, RO 3550/16-1, WE 5707/2-1; Dr. Ernst-Leopold Klipstein Foundation

KEYWORDS
AGO, Argonaute, DCL, Dicer-like, RNAi

1 | INTRODUCTION

RNA interference (RNAi) is a conserved mechanism that regulates gene expression via small (s)RNAs (Huang et al., 2019; Tang et al., 2022), which can be classified into micro (mi)RNAs (20–22 nt) and small interfering (si)RNAs (21–24 nt). In the interaction with infectious agents, host sRNAs target foreign genes to mediate defense, e.g., against viruses (Obbard et al., 2008; Zhan & Meyers, 2023). Host sRNAs also fine-tune the expression of host immune-responsive genes, thereby orchestrating the outcome of infection against various pathogens (Šečić, Kogel, & Ladera-Carmona, 2021). For example, in the genetic model *Arabidopsis thaliana*, miRNA393 enhances resistance to *P. syringae pv. tomato* strain DC3000 (*Pto* DC3000) by regulating pattern-triggered immunity (PTI) through auxin signaling suppression (Navarro et al., 2006). During seedling development, miR172 inhibits the expression of FLAGELLIN SENSING2 (FLS2), a well-studied pattern recognition receptor (PRR) that confers PTI against flagellated bacteria (Zou et al., 2018). This suggests a role of miR172 in coordinating plant immunity and development.

The core mechanism of RNAi involves the production of dsRNAs, which are processed into sRNA duplexes by DICER-LIKE (DCL) proteins. These sRNAs are subsequently loaded into RNA-induced silencing complexes (RISCs) (Iwakawa & Tomari, 2022; Martín-Merchán et al., 2023). To amplify RNAi, RNA-dependent RNA polymerases use single-stranded sRNA to generate long dsRNAs, which are processed by DCL2/DCL4 into secondary-phased siRNAs (Curaba & Chen, 2008; Martín-Merchán et al., 2023). *A. thaliana* encodes four DCL proteins, each producing specifically sized sRNAs (Martín-Merchán et al., 2023), suggesting specific functions. A partial *DCL1* loss-of-function mutant in *A. thaliana* showed enhanced susceptibility to *Pto* DC3000 and *Botrytis cinerea* infection (Navarro et al., 2006; Weiberg et al., 2013), but also displayed developmental abnormalities. DCL2 and DCL4 mediate antiviral immunity (Taochy et al., 2017; Z. Wang et al., 2018) (Azevedo et al., 2010; Bouché et al., 2006; Deleris et al., 2006). DCL4 is also crucial for anti-fungal defense since *dcl4* mutants showed increased susceptibility to the vascular fungus *Verticillium dahliae* (Ellendorff et al., 2009).

ARGONAUTE (AGO) proteins are key components of RISCs, bind single-stranded sRNAs, and guide them to sequence-complementary RNA and DNA targets (Fang & Qi, 2016). Ten AGO proteins have been identified in *A. thaliana* that can be classified into three clades: i) AGO1/5/10 (clade I), ii) AGO2/3/7 (clade II), and iii) AGO4/6/8/9 (clade III) (Martín-Merchán et al., 2023). They feature different subcellular localization patterns and sRNA binding preferences. The expression patterns of *AGO* genes do not seem to correlate with their clade assignment and function. The members of clade I and clade III, *AGO1* and *AGO4*, are ubiquitously expressed across tissues and during various developmental stages of *A. thaliana* (Jullien et al., 2022). The expression of *AGO2* and *AGO3* is induced in response to diverse abiotic and biotic stresses (Martín-Merchán et al., 2023). For example, *AGO2* expression is upregulated during *Pto* DC3000 infection (Zhang et al., 2011).

Several studies have examined the roles of AGO proteins in plant immunity against eukaryotic and prokaryotic microbes. For example, specific partial loss-of-function mutants in *AGO1* are compromised in microbe-associated molecular pattern (MAMP)-induced immunity against *Pto* DC3000 (Li et al., 2010). Since infection with the fungal pathogen *Sclerotinia sclerotiorum* showed more severe necrotic disease symptoms in *ago1* mutants (Cao et al., 2020), the study suggests that AGO1 is a positive regulator of PTI and enhances resistance against *S. sclerotiorum*. However, AGO1 has also been described to negatively regulate plant immunity against the fungal pathogens *B. cinerea*, *V. dahliae*, *V. longisporum* and *Botryosphaeria dothidea*, as well as the oomycete *H. arabidopsidis* (Dunker et al., 2020; Ellendorff et al., 2009; Shen et al., 2014; Weiberg et al., 2013; Yu et al., 2017). Yet, AGO1 had no detectable role in the outcome of infection with the fungal and oomycete pathogens *Erysiphe cruciferarum* and *Albugo laibachii*, respectively (Dunker et al., 2020). Of the other clades, Arabidopsis *ago2* mutants are more susceptible to infection by *V. dahliae*, *S. sclerotiorum*, and species of the oomycete pathogen *Phytophthora* (Cao et al., 2020; Ellendorff et al., 2009; Guo et al., 2018). Furthermore, AGO4 contributes to resistance to *Pto* DC3000 and is required for both local and *Trichoderma*-induced systemic immunity against *B. cinerea* (Agorio & Vera, 2007; López et al., 2011; Rebolledo-Prudencio et al., 2022).

AGO proteins act together with their loaded sRNAs within the RISC complex, suggesting that the above-outlined examples of immunity regulation in *A. thaliana* likely depend on the specificity of the sRNAs. Beyond the evolution of pathogen-derived molecular suppressors that interfere with host RNAi (Hou et al., 2019; Navarro et al., 2006), infectious microbes can hijack host AGO1 and incorporate microbe-derived sRNAs to facilitate infection. This cross-kingdom (ck)RNAi has been demonstrated for the interaction of *A. thaliana* with the taxonomically diverse pathogens *B. cinerea* and *H. arabidopsidis* (Dunker et al., 2020; Weiberg et al., 2013). In both cases, it is mediated by fungal- or oomycete-derived sRNAs, respectively, which are loaded into host AGO1 and thereby interfere with host RNAi pathways. Supporting this, the *B. cinerea rdr1 and dcl1/dcl2* mutants were less virulent on both *A. thaliana* and *Solanum lycopersicum* hosts, since the production of sRNAs was nearly abolished in these fungal mutants (Cheng et al., 2023; Weiberg et al., 2013). Since plants also deliver sRNAs into *B. cinerea* (Cai et al., 2018), ckRNAi occurs in both directions of the interacting organisms.

Different *B. cinerea* genotypes exhibited varied infection phenotypes (Qin et al., 2023; Weiberg et al., 2013). Hence, the contribution of RNAi to the outcome of microbial infections tends to be more complex and possibly species- or even pathotype-dependent. Therefore, it cannot always be assumed with certainty that plant mutants in the RNAi pathway exhibit phenotypes at each time point when infected with any microbe. To address this aspect in a broader taxonomic context, we characterized the expression patterns and loss-of-function mutant phenotypes of an informative set of *DCL* and *AGO* genes upon infection with a panel of pathogenic filamentous microbes and bacteria, each with different lifestyles, including mutualistic colonization. We reproduced some previously investigated phenotypes and uncovered new roles for AGO1, AGO2, AGO4, and AGO10 in certain microbial interactions, specifically, the dual role of AGO1 as both a positive and negative regulator of plant immunity. This study provides a phenotypic framework for the context-dependent regulatory function of *DCL* and *AGO* genes in plant immunity, offering insights into how plants dynamically adjust their defense strategies to different types of microbial interactions.

2 | RESULTS

We selected a set of *A. thaliana* genes and their corresponding mutants that are informative for the siRNA pathway. These include *DCL2*, *DCL3*, *DCL4* and the triple *dcl2/3/4* mutant and members of the three AGO clades (*AGO1*, *AGO10*, the *ago1–27*, *ago1–46* and *ago10–1* mutants (clade I), *AGO2* and the *ago2–1* mutant (clade II), *AGO4* and the *ago4–2* mutant (clade III) (Table S1). Exploring publicly available transcriptome data of *A. thaliana* elicited with MAMPs from fungi (ch8, nlp20), oomycete (nlp20), and bacteria (flg22, elf16, LPS, nlp20) (Bjornson et al., 2021), we noted that all tested *AGO* but not the selected *DCL* genes were responsive to the immune stimuli (Figure S1). Of the *AGO* genes, *AGO2* showed upregulation in response to all MAMPs, while *AGO1*, *AGO4*, and *AGO10* were downregulated in response to bacterial MAMPs. This suggests that *AGO* genes across the three clades could be involved in PTI regulation. The strong MAMP-induced expression of *AGO2* is consistent with its documented role in immunity against the pathogenic fungus *S. sclerotiorum* and anti-bacterial immunity against *Pto* DC3000 and its AvrRpt2-avirulent derivative (Cao et al., 2020; Zhang et al., 2011).

Since *AGO* gene expression was responsive to MAMPs derived from different microbial taxa, we selected a panel of pathogenic fungi (*Thecaphora thlaspeos*, *E. cruciferarum*, *V. longisporum*), a symbiotic fungus (*Serendipita indica*), and bacterial pathogens (*Pto* DC3000, *X. campestris* pv. *campestris*, *Xylella fastidiosa* subsp. *fastidiosa*) to study the *DCL* and *AGO* expression profiles as well as the infection phenotypes of corresponding mutants in *A. thaliana* (Table S2). We also included an oomycete pathogen (*H. arabidopsidis*), given that AGO1-dependent ckRNAi has been demonstrated to play a role in its infection outcome in *A. thaliana* (Dunker et al., 2020). The selected microbes also differ in their lifestyles, with *H. arabidopsidis* and *Pto* DC3000 infecting leaf mesophyll tissue, *E. cruciferarum* invading leaf epidermal cells, *S. indica* colonizing roots, and *V. longisporum*, *X. campestris* pv. campestris and *X. fastidiosa* infecting the plant xylem, and *T. thlaspeos* growing systemically along the vasculature in both roots and aerial tissues (Table S2). Appreciating the diverse lifestyles, we performed the infection experiments tailored to the type of plant-microbe interaction and according to well-established protocols, yet mainly at the whole plant/organ scale with in vitro and soil-grown plants. Gene expression was analyzed at different time points in the early, middle, and late infection/colonization stages depending on the interacting microbe. The infection/colonization success was measured as the ability to invade host cells (number of penetration events), as microbial biomass (number of hyphae or microbial DNA/RNA), scoring of the infection progress, or as the capacity of the microbe to multiply within host tissue (number of colony-forming units [cfu]). To minimize the putative effect of seed batches, we used an age-matched seed collection of *A. thaliana* Col-0 and the selected *dcl2/3/4* and *ago* mutants for our experiments.

2.1 | AGO1 is a regulator of immunity against some but not all filamentous pathogens

We first tested our collection of plant lines and investigated the role of *DCL* and AGO proteins in the interaction with *H. arabidopsidis*. Expression of *DCL2*, *DCL4*, and *AGO2* was upregulated at middle (4 days post inoculation [dpi]) and late (6 dpi) stages of *H. arabidopsidis* infection, while *AGO4* was downregulated at these time points (Figure 1a). This is in agreement with the changes in the expression of *AGO2* and *AGO4* in response to the oomycete MAMP nlp20 (Figure S1). No drastic changes in gene expression were observed for *AGO1* and *AGO10* (Figure 1a). In the infection experiments, *ago1–27* and *ago1–46* mutants displayed enhanced resistance to *H. arabidopsidis* at 6 dpi (Figure 1b). No altered infection was observed in *ago2–1* and *ago4–2* mutants. This outcome is consistent with a previous report showing evidence for loading pathogen-derived sRNAs into *A. thaliana* AGO1, resulting in ckRNAi to support infection (Dunker et al., 2020). Collectively, the data suggests a specific role for AGO1 in the interaction with the oomycete pathogen.

AGO1 also negatively regulates immunity against fungal pathogens including, *B. cinerea* and *V. longisporum* but not *E. cruciferarum* (Dunker et al., 2020; Shen et al., 2014; Weiberg et al., 2013). Consistent with the fact that AGO1 negatively regulates immunity against *V. longisporum* (Shen et al., 2014), *AGO1* expression was downregulated in the course of infection with this fungal pathogen (Figure S2). By contrast, *DCL3* and *DCL4* were upregulated by *V. longisporum*, suggesting a different response to this pathogen.

Next, we explored the selected *DCL* and *AGO* genes for their expression profiles in response to the challenge with *E. cruciferarum*. We found reduced *AGO1*, *AGO4*, and *AGO10* expression and upregulation of the tested *DCL* genes across the time course (Figure 2a). Fungal entry rates were slightly, yet statistically significantly, increased in *ago1–27*, but no differences were observed in any of the other tested mutants, including the allelic *ago1–46* mutant (Figure 2b). This outcome

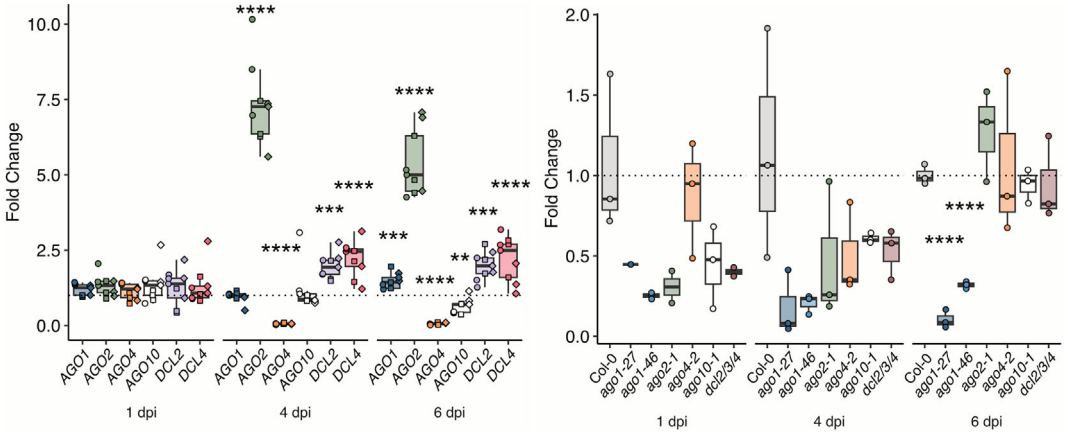

FIGURE 1 *DCL* and *AGO* gene expression patterns (a) and colonization in respective mutants (b) upon infection with *H. arabidopsidis* isolate Noco 2. (a) Samples were collected at 1 dpi (days post inoculation), 4 dpi, and 6 dpi. The RNA levels are relative to mock and normalized against *CDKA*. The results of three biological replicates are depicted. (b) Pathogen load on *ago* and *dcl* mutants was assessed by measuring relative *H. arabidopsidis* gDNA quantities with RT-qPCR at 1 dpi, 4 dpi, and 6 dpi. The result of one biological replicate is depicted. Error bars show standard deviation. Statistical significance was assessed by two-sided Welch's *t*-test ($\alpha = .05$, *p*-values * < .05, ** < .01, *** < .001, **** < .0001). Symbols indicate number of biological replicates. Circle = first, square = second, diamond = third. The dashed line indicates a fold change = 1.

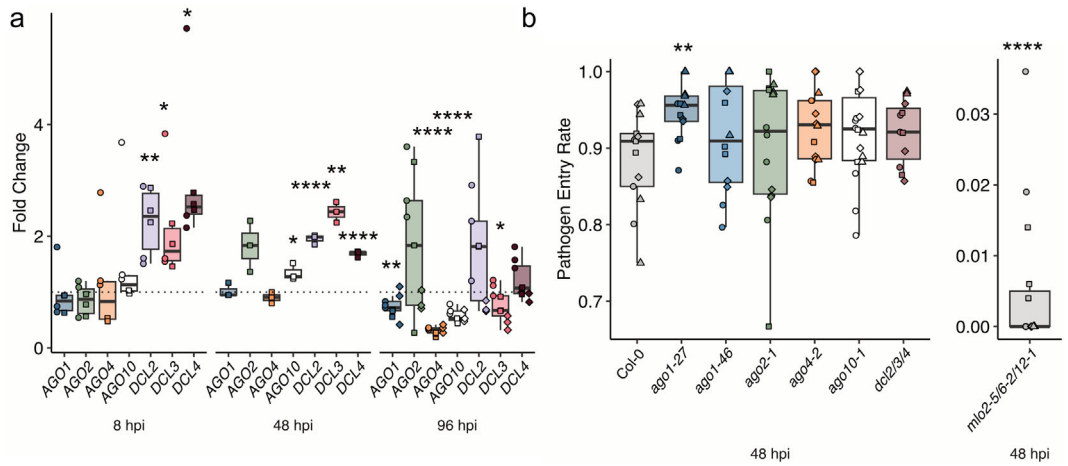

FIGURE 2 *DCL* and *AGO* gene expression patterns (a) and colonization in respective mutants (b) upon *E. cruciferarum* infection in a time course experiment. (a) Samples were collected at 8 hpi (hours post inoculation), 48 hpi, and 96 hpi. The RNA levels are relative to mock and normalized against *CDKA*. The results of three biological replicates are depicted. (b) Infection success on *ago* and *dcl* mutants was assessed by determining *E. cruciferarum* host cell entry rates at 48 hpi. The results of four biological replicates are depicted. Error bars show standard deviation. Statistical significance was assessed by two-sided Welch's *t*-test ($\alpha = .05$, *p*-values * < .05, ** < .01, *** < .001, **** < .0001). Symbols indicate number of biological replicates. Circle = first, square = second, diamond = third, triangle = fourth. The dashed line indicates a fold change = 1.

confirms previous data on unaltered *E. cruciferarum* infection in *ago1–46*. However, it contrasts the reported wild type-like phenotype in *ago1–27* (Dunker et al., 2020) possibly due to different scoring: the previous study evaluated leaf necrosis, while in our study, fungal penetration was scored. Furthermore, a clear regulation of *E. cruciferarum* penetration success by AGO1 cannot be established, since the two *ago1* mutants exhibited different infection phenotypes to this fungus (Figure 2b). We also investigated the role of AGO1 during infection with *T. thlaspeos* and observed wild-type-like colonization in *ago1–27* mutants (Figure 3). By contrast, *ago4–2* mutants showed significantly enhanced susceptibility, thereby revealing a previously unknown role for AGO4 as a positive regulator of immunity to this smut fungus.

2.2 | AGO1 is a regulator of certain but not all bacterial infections

Motivated by the previous reports on the roles of AGO1 and AGO2 in immunity against bacterial pathogens (Ren et al., 2019; Zhang et al., 2011), we examined the roles of the selected *DCL* and *AGO* genes in infection by three different bacterial pathogens. Interestingly, AGO1 might be required for immunity against *X. fastidiosa*, since it was upregulated at late infection stages (Figure 4a), and both *ago1–27* and *ago1–46* displayed enhanced susceptibility (Figure 4b). All other tested genes showed wild-type-like expression patterns, and the respective mutants supported wild-type-like infection success of *Pto* DC3000

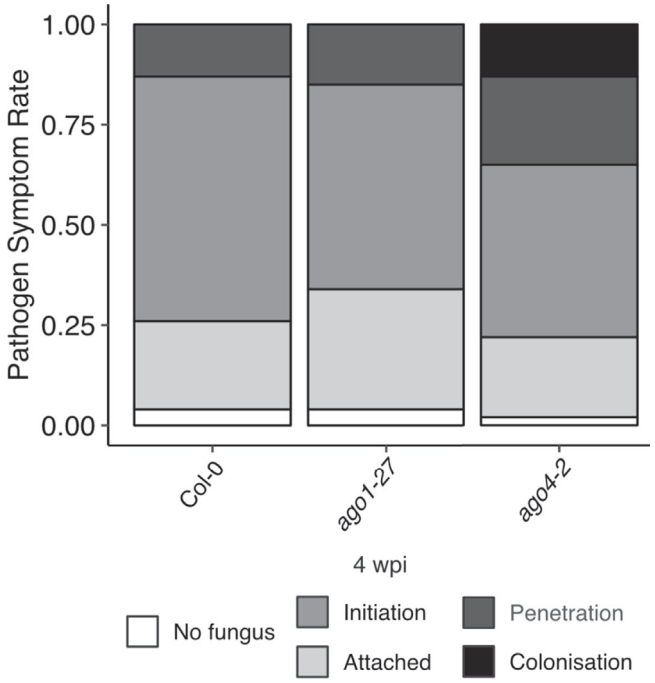

FIGURE 3 Colonization in *ago* mutants upon *T. Thlaspeos* infection. Colonization was visualized after four weeks by staining with wheat germ agglutinin (WGA, fungal hyphae) and propidium iodide (PI, plant background). In at least 150 seedlings per line, fungal progression was classified into (i) attachment of the fungus to plant tissue, (ii) initiation of penetration as indicated by bulging of the hyphal tip, (iii) penetration into the plant tissue, and (iv) colonization along the vasculature. Similar results were obtained in three independent experimental replicates.

(Figure S3A and S3B) and *X. campestris* pv. *campestris* (Figure S4A and S4B). The tested bacteria are Gram-negative γ-proteobacteria, including two belonging to the Xanthomonadaceae and colonizing xylem vessels (Table S3). However, the positive regulatory function of AGO1 appears to be specific to immunity against *X. fastidiosa*.

Previously, AGO2 and AGO4 were shown to positively regulate immunity against *Pto* DC3000 strains (Agorio & Vera, 2007; López et al., 2011; Zhang et al., 2011), which is not consistent with our findings. We neither detected any obvious induction of *AGO2* expression nor increased *Pto* DC3000 susceptibility in *ago2* and *ago4* mutants (Figure S3). It is possible that the different outcomes for these mutants might depend on the methods of bacterial inoculation, as in the previous studies, bacteria were applied by syringe-based leaf infiltration, while in this study, *Pto* DC3000 was sprayed onto the leaf surface. The two inoculation methods differ, as syringe inoculation bypasses stomatal immunity (Melotto et al., 2017).

2.3 | AGO2 and AGO10, but not AGO1, are potential regulators of fungal mutualism

Soybean AGO1 plays a positive role in the bacterial *Sinorhizobium* root-nodule symbiosis via ckRNAi (Ren et al., 2019). Furthermore, AGO1 has been speculated to regulate fungal symbiosis, supported by the prediction of plant mRNA targets of fungal sRNAs accumulating in the symbiosis between beneficial microorganisms and their hosts (Silvestri et al., 2019; Valdés-López et al., 2019; Wong-Bajracharya et al., 2022). Therefore, we next conducted colonization experiments with the mutualist basidiomycete *S. indica*, revealing *AGO4* downregulation at late time points (Figure 5a). The other tested *DCL* and *AGO* genes revealed no statistically significant changes in response to *S. indica* colonization at the investigated time points (Figure 5a). Interestingly, roots of *ago2–1* and *ago10–1* mutants showed reduced colonization by *S. indica*, whereas *ago1–27*, *ago4–2*, and *dcl2/3/4* exhibited wild type-like colonization (Figure 5b). It suggests that AGO2 and AGO10, but not AGO1, function as potential positive regulators during colonization in the mutualistic interaction of *A. thaliana* with *S. indica*, or negatively regulate immunity against this beneficial fungus. Moreover, although clade I AGO1 and AGO10 are phylogenetically related, AGO10 may have a specific function in fungal mutualism. Of note, miRNAs can be sequestered by different AGO proteins, leading to different outcomes, e.g., as shown for miRNA165/166 in flower development, which depends on their binding to AGO1 and AGO10 (Ji et al., 2011).

2.4 | AGO expression patterns do not seem to correlate with their function in immunity

We utilized heat maps to summarize our mutant infection and gene expression data. Overall, some of the most striking phenotypes were associated with *ago1*, *ago2*, and *ago10* mutants: *ago1* mutants were more susceptible to *X. fastidiosa* but more resistant to *H. arabidopsidis* while *ago2* and *ago10* were more resistant to *S. indica* (Figure 6a). Yet, despite these notable phenotypes, the overall gene expression patterns did not correlate with the mutant infection data (Figure 6b). The most striking changes in gene expression were observed for *AGO2* and *AGO4*, showing up- and down-regulation upon *H. arabidopsidis* infection, respectively (Figure 6b). *AGO4* and *AGO10* were also down-regulated in response to *E. cruciferarum*. This suggests distinct underlying mechanisms or pathways influencing the observed phenotypic outcomes.

3 | DISCUSSION

RNAi executed by DCL and AGO proteins is considered a conserved process regulating the outcome of plant-microbe interactions. Previous studies have described the roles of AGOs as positive and negative plant immunity regulators, likely linked to their binding of host or pathogen-derived sRNAs. Here, we i) confirm previous findings for AGO1 in negatively regulating immunity against *H. arabidopsidis* (Figure 1b) and ii) reveal a potential positive regulatory role of AGO1 in immunity against *X. fastidiosa* (Figure 4b). Moreover, iii) we identified clade I AGO10 and clade II AGO2 as positive modulators of *S. indica* root colonization (Figure 5b), and iv) revealed clade III AGO4

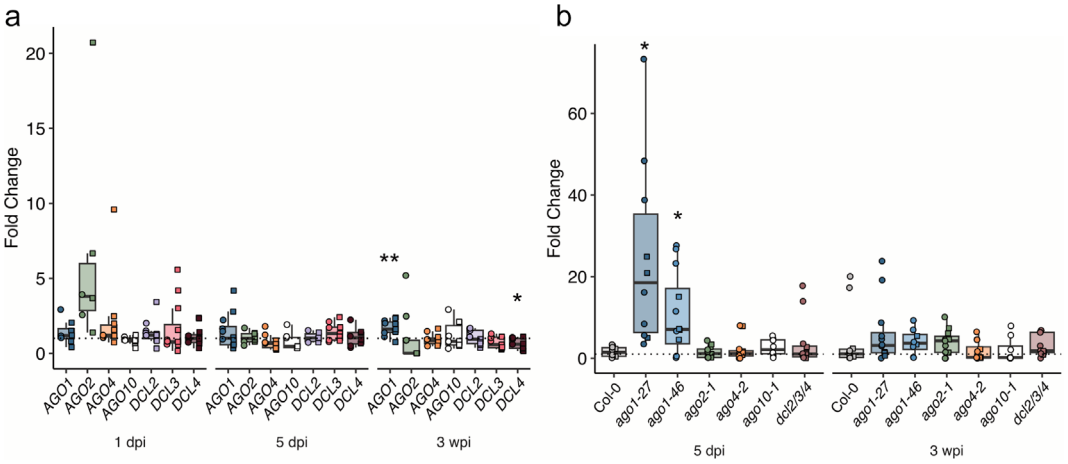

FIGURE 4 *DCL* and *AGO* gene expression patterns (a) and colonization in respective mutants (b) upon *Xylella fastidiosa subsp. fastidiosa* Temecula1 infection. (a) Samples were collected from petioles at 1 (day post-infection), 5 dpi, and 3 wpi (weeks post-infection). The RNA levels are relative to mock and normalized against *CDKA*. The results of two biological replicates are depicted. (b) Pathogen load on *ago* and *dcl* mutants was assessed by RT-qPCR at 5 dpi and 3 wpi. The results of two biological replicates are depicted. Error bars show standard deviation. Statistical significance was assessed by two-sided Welch's *t*-test ($\alpha = .05$, *p*-values * < .05, ** < .01, *** < .001, **** < .0001). Symbols indicate number of biological replicates. Circle = first, square = second, diamond = third. The dashed line indicates a fold change = 1.

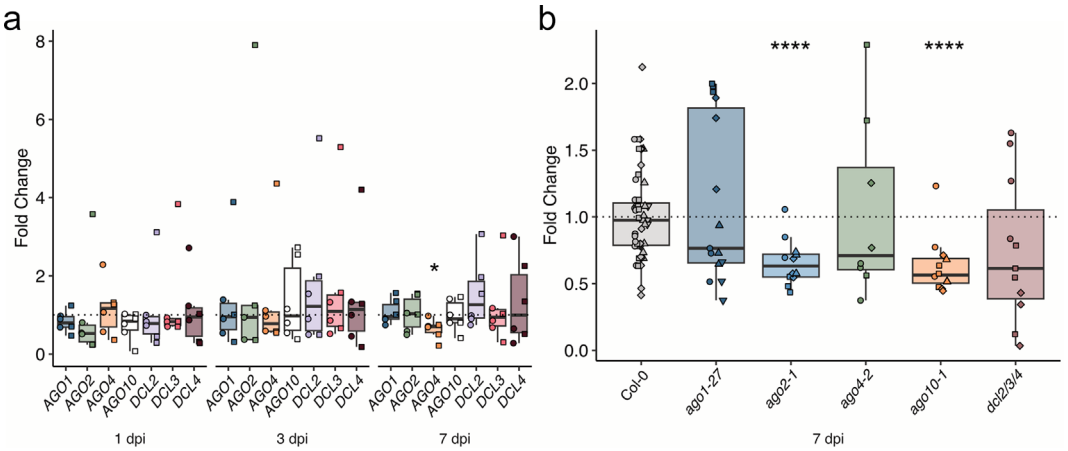

FIGURE 5 *DCL* and *AGO* expression patterns (a) and colonization in respective mutants (b) upon infection with *S. indica*. (a) Samples were collected from roots at 1 dpi (day post inoculation), 3 dpi, and 7 dpi. The RNA levels are relative to mock and normalized against *UBC21*. The results of two biological replicates are depicted. (b) Pathogen load on *ago* and *dcl* mutants was assessed by measuring relative *S. indica* gDNA quantities with RT-qPCR at 7 dpi. The results of at least three biological replicates are depicted. Error bars show standard deviation. Statistical significance was assessed by two-sided Welch's *t*-test ($\alpha = .05$, *p*-values * < .05, ** < .01, *** < .001, **** < .0001). Symbols indicate number of biological replicates. Circle = first, square = second, diamond = third. The dashed line indicates a fold change = 1.

as a positive control element of *T. thlaspeos* infection (Figure 3). Thus, our broad-scale phenotyping uncovered previously unknown positive and negative regulatory functions of different AGO proteins in the context of plant-microbe interactions (Figure 6c).

AGO1's negative adjustment of plant immunity is influenced by its role as a target for pathogen-derived sRNAs and its function in ckRNAi (Dunker et al., 2020; Weiberg et al., 2013). Therefore, it is possible that AGO1-related AGO10 and AGO2 might be hijacked by *S. indica*-secreted sRNAs, providing a possible molecular mechanism of their positive modulatory role in mutualism with this fungus. Indeed, the production of host and fungal-derived sRNAs has been revealed in the beneficial interaction of *Brachypodium distachyon* with *S. indica* (Šečić, Zanini, et al., 2021), which could result in post-transcriptional gene silencing (PTGS) of plant immunity genes and thereby facilitating *S. indica* colonization. This scenario is consistent with AGO1's role in bacterial symbiosis, binding rhizobial tRNA-derived sRNA fragments (tRFs) that promote host nodulation (Ren et al., 2019). Additionally, clade I AGOs could influence the host's transcriptional response to symbiosis, as reported for AGO5 in rhizobia-*Phaseolus vulgaris* symbiosis (del Sánchez-Correa et al., 2022).

A positive immune regulatory function of AGO proteins has been linked to its binding of host endogenous sRNAs. For example, miR393b* bound to AGO2 triggers *MEMB12* (encoding a Golgi-localized SNARE protein) cleavage, which results in increased

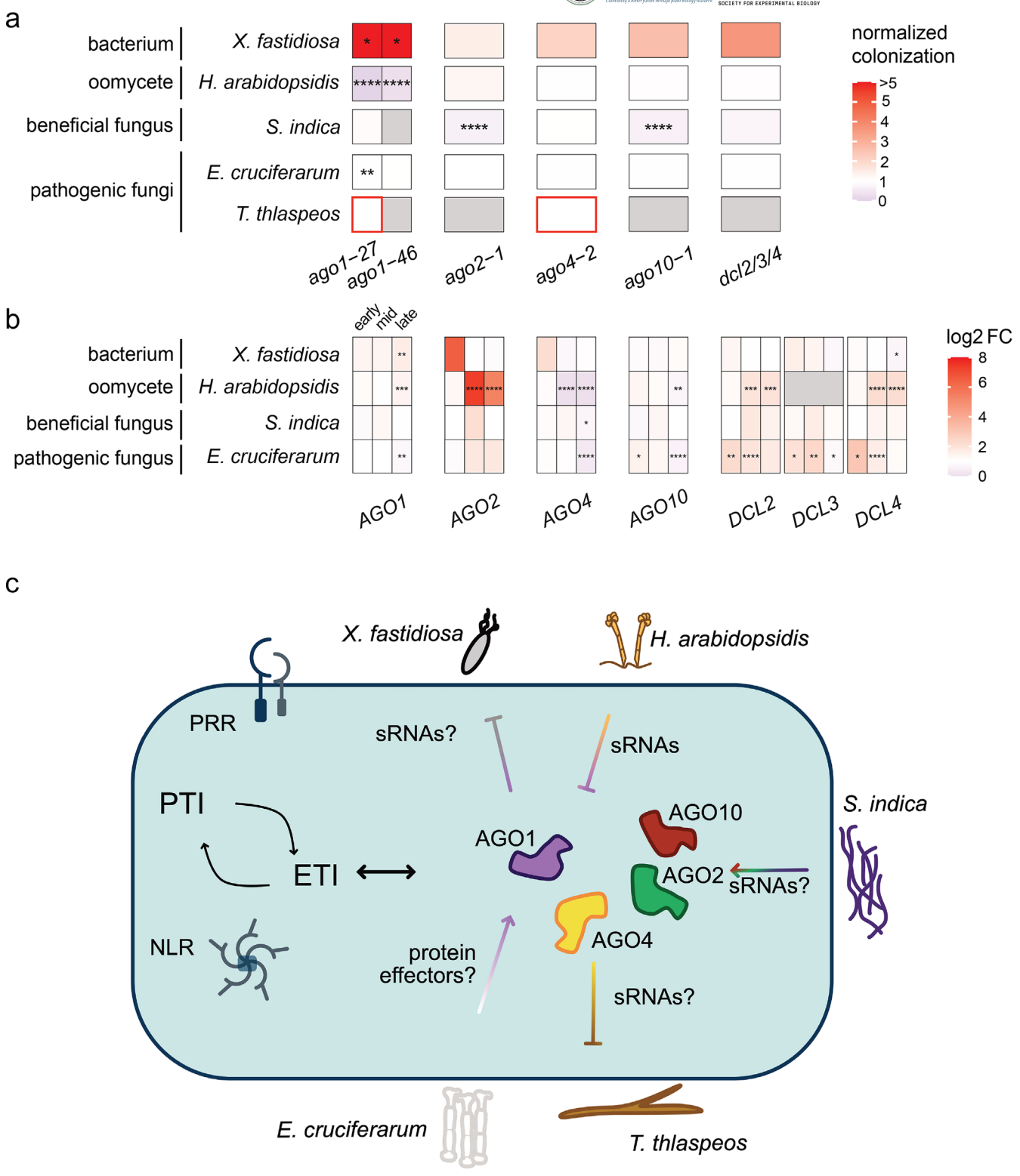

FIGURE 6 Legend on next page.

FIGURE 6 Overall results presented in heat maps and a graphical summary. (a) The heat map shows the colonization success of *S. indica*, *Xylella fastidiosa*, *T. thlaspeos*, *H. arabidopsidis*, and *E. cruciferarum* in the set of selected Arabidopsis mutants (*ago1*–27, *ago1*–46, *ago2*–1, *ago4*–2, *ago10*–1, *dcl2/3/4*) at 7 dpi, 5 dpi, 2 dpi, 6 dpi, and 2 dpi, respectively to the interacting microbe. Color intensity within each cell represents the degree of colonization success relative to wild-type Col-0 plants, with red indicating more colonization and blue indicating less colonization. Significant differences are marked with asterisks ($\alpha = .05$; adjusted *p*-values: * < .05, < .01, * < .001, **** < .0001). Non-quantifiable colonization success in *T. thlaspeos* is indicated as red boxes to indicated increased colonization. (b) Transcript abundance as log2 (fold change) of the genes of interest (*AGO1*, *AGO2*, *AGO4*, *AGO10*, *DCL2*, *DCL3*, *DCL4*) was assessed at an early, mid, or late infection stage in Col-0 for each microbe. Color intensity within each cell corresponds to the change in gene expression relative to non-inoculated samples, with red indicating upregulation and blue indicating downregulation. Significant differences are indicated with asterisks ($\alpha = .05$, adjusted *p*-values * < .05, < .01, * < .001, **** < .0001). Non-tested conditions are indicated as gray boxes. (c) Proposed model. Potential cross-talk between the plant immune system and the RNA interference pathway influenced by different microbes. Key components of the plant immune system include pattern recognition receptors (PRRs) mediating pattern-triggered immunity (PTI) and nucleotide-binding leucine-rich repeat receptors (NLRs) involved in effector-triggered immunity (ETI). Microbes such as *X. fastidiosa*, *Hyaloperonospora arabidopsidis*, *Serendipita indica*, *Tecaphora thlaspeos*, and *Erysiphe cruciferarum* may interact with the plant immune system indirectly via Argonaute (AGO) proteins. This modulation can occur bidirectionally and might be mediated by small RNAs (sRNAs) and/or effector proteins, depending on the specific microbe involved. The arrows indicate hypothesized relationships based on the presented data.

resistance due to the secretion and accumulation of the Pathogenesis-Related (PR) 1 protein (Zhang et al., 2011). A potential function of AGO1 in restricting *X. fastidiosa* infection may be related to endogenous host sRNAs associated with the control of PTI or its execution (Mitre et al., 2021; Navarro et al., 2006; Zhang et al., 2011). Given that ckRNAi functions in both directions (Cai et al., 2018), plants may also send AGO1-dependent sRNAs to alter *X. fastidiosa* growth, interfering with gene silencing in bacteria (Papenfort & Melamed, 2023).

The identification of AGO4 as a positive control element of resistance to *T. thlaspeos* expands the importance of this AGO protein beyond its requirement for immunity against *Pto* DC3000 and *B. cinerea* (Agorio & Vera, 2007; Rebolledo-Prudencio et al., 2022). Of note, upon infection with *Blumeria graminis* f.sp. *tritici*, *AGO4* was significantly downregulated in the wheat progenitor *Aegilops tauschii*, which was accompanied by a substantial reduction in AGO4a-sorted 24-nt siRNA levels, and enrichment for 'response to stress' gene functions, including receptor kinase, peroxidase, and pathogenesis-related genes, suggesting that AGO4 in some cases is a strong negative regulator of immunity (Geng et al., 2019). It further highlights the involvement of clade III AGOs-mediated TGS in the modulation of plant immunity. Interestingly, AGO1 was not required for *T. thlaspeos* infection at the early stages of colonization. Other AGOs of clade I and clade II need to be investigated to address the putative role of PTGS in this fungal interaction during the established biotrophic phase or during fungal sporulation.

The other tested interactions did not reveal obvious phenotypes. This was unexpected given the functional conservation of AGOs and the ubiquitous expression of key members like *AGO1* and *AGO4* in most tissues, including leaves, roots, and the vasculature (Martín-Merchán et al., 2023; Wook et al., 2011). The transcriptional response of *DCL* and *AGO* genes was mostly not correlated with infection phenotypes in respective mutants. Considering the different infection types, from epidermal (*E. cruciferarum*), leaf mesophyll (*H. arabidopsidis*,, *Pto* DC3000), root (*S. indica*) to vascular tissues (*V. longisporum*, *X. campestris* pv. *campestris*, *X. fastidiosa*, *T. thlaspeos*), a spatiotemporal resolution might be needed to observe changes in gene expression at the actual site of pathogen colonization (Dunker et al., 2020). We speculate that functional redundancy within the DCL and AGO family is likely accounting for wild-type-like phenotypes in some of the tested interactions. This includes the *dcl2/3/4* triple mutant, therefore suggesting potential further redundancy of these three encoded proteins with DCL1. Moreover, infection with *E. cruciferarum* and *X. campestris* pv. *campestris* did not reveal infection phenotypes in the tested mutants (Figure 2b and Figure S4B). This could suggest more functional redundancies among AGO proteins than expected.

To a large extent, the outcome of infection success is determined by the ability of the pathogen to suppress host immunity (Jones et al., 2024). This capacity is encoded in the pathogen's repertoire of diverse molecular effectors (Y. Wang et al., 2022). For example, the virulence of bacterial pathogens like *Pto* DC3000 and *X. campestris* pv. *campestris* mainly involves Type-3-secreted effector proteins (Y. Wang et al., 2022). *X. fastidiosa* lacks a Type-3 secretion system (Landa et al., 2022), and immune-suppressing protein effectors have not been described to date. Thus, the bacterium might not be able to overcome AGO1-mediated defenses. Effector proteins have also been demonstrated to improve infection of powdery mildew fungi such as *E. cruciferarum* (Bourras et al., 2018). It is, therefore, possible that protein effectors could be largely responsible for virulence in a given microbe, contrasting to the virulence mechanisms of *B. cinerea* and *H. arabidopsidis*, which at least in part rely on sRNA-like effectors (Dunker et al., 2020; Weiberg et al., 2013). Moreover, protein effectors could suppress host RNAi (Hou et al., 2019; Navarro et al., 2006). Since pathotypes of microbial subspecies encode different effector repertoires, their interaction with the host's RNAi machinery might differ (Qin et al., 2023; Weiberg et al., 2013).

To conclude, analyzing the role of RNAi in plant immunity across taxonomically diverse microbes may be more complex and might need refined experimental set-ups beyond whole plant phenotyping with improved spatiotemporal resolution. We consider three levels of functional redundancy, which complicate the phenotypic analysis: i) similar or overlapping functions of DCL and AGO clade members, ii) microbial virulence conferred by protein effectors, including iii) microbial protein effectors suppressing host RNAi. Therefore, experimental studies would benefit from using higher-order plant mutants (if not exhibiting severe

developmental phenotypes) and combinatorial analysis with different pathotypes of microbial (sub-)species, as well as microbial mutants compromised e.g. for selected protein effectors or their secretion. Taken together, this phenotypic framework will now make it possible to dissect the molecular mechanisms by which AGOs function, whether host sRNAs modulate the plant's immune system, are secreted to function in the microbe, or if microbe-derived sRNAs are delivered into the plant. Ultimately, this will allow improvement of plant protection.

4 | MATERIAL AND METHODS

4.1 | Plant materials

A. thaliana Col-0 mutants included published *ago1–27*, *ago1–46*, *ago2–1*, *ago4–2*, *ago10–1*, and *dcl2/3/4* (Table S1). Age-matched seeds were used for all experiments. The *eds1–2* mutant was used for propagation of the *E. cruciferarum* inoculum, and the *mlo2–5/6–2/12–1* mutant as an additional control for powdery mildew infection experiments (Bartsch et al., 2006; Consonni et al., 2006).

4.2 | Primers

All primers used in this study are listed in Table S3. The *CDKA* gene expression was used as a reference to assess the expression levels of the selected *AGO/DCL* genes and to quantify microbial growth *in planta* (*H. arabidopsidis*, *X. fastidiosa*) by (RT)-qPCR. For *S. indica* colonization, *UBC21* was used as a reference gene.

4.3 | Microbial infections

4.3.1 | *Hyaloperonospora arabidopsidis*

Plants for infection with *H. arabidopsidis* (GÄUM.) isolate Noco 2, *A. thaliana* plants were grown on soil under long day conditions (16 h light, 8 h dark, 60% relative humidity). Two weeks-old *A. thaliana* plants were inoculated with a final spore concentration of $2*10^4$ spores mL^{-1} as previously described (Ried et al., 2019). For biomass quantification, two leaves and two cotyledons were pooled for one technical replicate, followed by genomic DNA extraction with CTAB and RNase A treatment (Promega) (Chen & Ronald, 1999). The isolated DNAs were diluted to 5 ng/µl. *H. arabidopsidis* gDNA relative to *A. thaliana* was quantified by qPCR with Primaquant low ROX qPCR master mix (Steinbrenner Laborsysteme) according to the manufacturer's instructions (95 °C 3 min, 95 °C 20 s, 60 °C 30 s, 72 °C 40 s, 40 cycles, and subsequent melting curve analysis).

For RT-qPCR, four leaves were pooled for one technical replicate. The CTAB method was used for total RNA extraction (Bemm et al., 2016). Genomic DNA was removed by DNase I digestion (Sigma-Aldrich) following the manufacturer's instructions. For cDNA synthesis with the Maxima H Minus Reverse Transcriptase (Thermo Fisher Scientific) kit, 1 µg of total RNA from each sample was used. Relative gene expression was quantified by qPCR with the Primaquant low ROX qPCR master mix (Steinbrenner Laborsysteme), according to the manufacturer's instructions (95 °C 3 min, 95 °C 20 s, 60 °C 30 s, 72 °C 40 s, 40 cycles, melting curve analysis).

4.3.2 | *Erysiphe cruciferarum*

Plants for *E. cruciferarum* infection were grown on SoMi 513 soil (Hawita, Vechta, Germany) in 9*9 cm pots under short-day conditions with an 8-h photoperiod at 22 °C and 16 h darkness at 20 °C. *E. cruciferarum* (in-house isolate of RWTH Aachen) was cultivated selectively on *A. thaliana eds1–2* (Bartsch et al., 2006) at 20 °C with an 8-h photoperiod. Spores from three pots of plants, collected at 20–28 dpi, were used for the inoculation of 10 pots. For this, four weeks-old healthy Col-0 plants, the selected mutant lines, and the resistant *mlo2–5/6–2/12–1* triple mutant (negative control) were placed in an inoculation tower and heavily infected inoculum plants were gently agitated to release spores. To determine fungal entry rates, for one technical replicate leaves from one plant were harvested at 48 hours post inoculation (hpi) and collected in 80% EtOH for de-staining of leaf pigments. Fungal structures were stained with Coomassie staining solution (45% MeOH (v/v), 10% acetic acid (v/v), .05% Coomassie blue R-250 (w/v)). Samples were double-blinded and leaves were analyzed by light microscopy. The fungal entry rate was determined as the percentage of spores successfully developing secondary hyphae over all spores that attempted penetration, visible by the presence of an appressorium (Kusch et al., 2019). At least 100 interaction sites on leaves of three different plants per independent replicate were analyzed.

For RT-qPCR, total RNA was extracted from leaves of uninoculated Arabidopsis and leaves sampled at 8, 48, or 96 hpi with *E. cruciferarum* using TRI reagent ® (Sigma Aldrich). For one technical replicate, each one leaf of three different plants was pooled. The remaining DNA was digested using DNase I (Thermo Fisher Scientific, USA). For cDNA synthesis, 1 µg RNA was used with the High-Capacity cDNA Reverse Transcription Kit (Applied Biosystems). Relative expression of target genes was quantified by RT-qPCR (95 °C 3 min, 95 °C 10 s, 60 °C 60 s; 40 cycles; melting curve analysis) with the Takyon no ROX SYBR 2X master mix (Eurogentec).

4.3.3 | *Verticilium longisporum*

Arabidopsis mutants used for *V. longisporum (VL43)* (Zeise & Von Tiedemann, 2002)infection were grown directly on soil in a climate chamber with 22 °C/18 °C day/night cycle with 8 h of light. For infection of mutant lines, an inoculation suspension was used. This suspension was prepared by flooding a fully grown three weeks-old culture of *V. longisporum* grown on Potato Dextrose Agar (PDA) agar (Carl Roth, Art. No. X931.1) in a Petri dish at 22 °C, in the dark with 10 ml ddH_2O. The Petri dish was scraped with a small metal spatula to release conidia in suspension. The suspension was filtered through miracloth

(Calbiochem, 475,855) to exclude mycelium, and spore concentration was determined using a hemocytometer (Thoma counting chamber - Marienfeld). The final concentration of the spore suspension was adjusted to 10.000.000 spores/mL. Two weeks-old seedlings of *A. thaliana* (Col-0 and mutant lines) were infected by pipetting 1 ml of inoculation suspension directly in the soil. For one technical replicate, leaf material from one plant was harvested 1, 7, and 35 dpi and ground on liquid nitrogen. Total RNA extraction was done using TRIzol® (Invitrogen) and Zymo RNA Clean & Concentrator-25 Kit with in-column DNase I digestion. cDNA synthesis was generated using 200 ng/µL of the extracted total RNA using RevertAid Reverse transcriptase (Thermo Scientific) following manufacturer guidelines. For subsequent qPCR, the SYBR™ Green PCR Master Mix (Applied Biosystems) was used (Thermo Fisher Scientific 4,309,155). For this, 10 µl reactions were set up, consisting of 5 µl SYBR master mix, .5 µl of each primer, 3.5 µl H_20, and .5 µl cDNA, run with 3 min of 95 °C followed by 40 cycles of 95 °C for 10s, 60 °C for 1 min, and subsequent melting curve analysis, on a QuantStudio 6 Flex (Applied Biosystems).

4.3.4 | *Thecaphora thlaspeos*

One seed of an Arabidopsis line was co-germinated with 300 sterilized teliospores of *T. thlaspeos* (collection 2022, Frantzeskakis et al., 2017) in 300 µl liquid half-strength Murashige and Skoog with Nitrate (MSN) medium (Duchefa) containing 1% sucrose in a well of a 96-well plate. The infections were incubated for four weeks in a light chamber for *A. thaliana* at long-day conditions (120 µE, 12 h 21 °C light, 12 h 18 °C darkness). Seedlings were then stained with wheat germ agglutinin (WGA) and propidium iodide (PI) as previously described (Frantzeskakis et al., 2017) and scored microscopically for fungal infection stages (Zeiss Axio Immager M1). Up to 160 seedlings, each representing one biological replicate, were inspected per line and experiment.

4.3.5 | *Serendipita indica*

A. thaliana mutant lines were grown on vertical square Petri dishes on *A. thaliana* Salt medium (ATS) (Lincoln et al., 1990) without sucrose and supplemented with 4.5 g/l Gelrite (Duchefa #G1101) in a 22 °C day/18 °C night cycle (8 h of light). Spores of *S. indica* (IPAZ-11827, Institute of Phytopathology, Giessen, Germany) were freshly isolated from the plates by scraping the agar using water supplied with .002% Tween 20 added and then filtered through miracloth (Merck Millipore), centrifuged at 3.000 x g for 7 min, then resuspended in water supplied with .002% Tween 20 and adjusted to 500.000 spores mL^{-1}. Roots of 14 days-old plants were inoculated with 1 ml of a suspension of 500.000 chlamydospores mL^{-1} in water with .002% Tween 20 per Petri dish. Control plants were treated with water supplied with .002% Tween 20 (mock). Inoculated roots of different mutants are harvested after seven days, and ground for 1 min at 30 Hz with the pre-cooled Retsch Mill (Tissue Lyser II, Retsch, Qiagen). For one technical replicate, roots from one plate were pooled. For quantification of *S. indica* colonization, genomic DNA was extracted using a Qiagen DNA extraction kit (QIAGEN, 69504). Fungal colonization was quantified using internal transcribed spacer (ITS) primers (see Table S3) and SYBR Green JumpStart Taq ReadyMix (Sigma Aldrich, 1,003,444,642) with a QuantStudio5 Real-Time PCR System (Applied Biosystems). A total of 2 µl ROX (CRX reference dye, Promega, C5411) were added to 1 ml SybrGreen as a passive reference dye that allows fluorescent normalization for qPCR data. The PCR conditions were 95 °C for 5 min followed by 40 cycles of 95 °C for 15 s, 60 °C for 30 s, and 72 °C for 30 s, followed by melting curve analysis.

For *DCL* and *AGO* gene expression, Arabidopsis Col-0 plants were grown on ATS plates and inoculated with *S. indica* spores as previously described above. Control plants were treated with water containing .002% Tween 20 (mock). Inoculated roots were harvested at 1, 3, and 7 dpi, ground with the tissue lyser, and RNA was extracted using Trizol and Zymo kit (Zymo research R2070), with a subsequent in-column DNase digestion. cDNA was generated from 1 µg RNA using Revert Aid Reverse transcriptase. Gene transcription was quantified by qPCR using SYBR Green JumpStart Taq ReadyMix (Sigma Aldrich, 1,003,444,642) with QuantStudio5 Real-Time PCR System (Applied Biosystems). A total of 2 µl ROX (CRX reference dye, Promega, C5411) were added to 1 ml SybrGreen as a passive reference dye that allows fluorescent normalization for qPCR data. The PCR conditions were 95 °C for 5 min, followed by 40 cycles of 95 °C for 15 s, 60 °C for 30 s, and 72 °C for 30 s, followed by a melting curve analysis. *Ubiquitin* (*UBC21*, *AT5G25760*) was used as a housekeeping gene for all experiments. Roots from two ATS plates were harvested and considered as one technical replicate. The results of three or more biological replicates are included in the data analysis.

4.3.6 | *P. syringae* pv. *tomato* DC3000

Plants for *Pto* DC3000 infection were grown on soil with 10 h light and 55% humidity for four to five weeks. *Pto* DC3000 was routinely grown at 28 °C on King's B plates with 1% Agar. Overnight plate-grown *Pto* DC3000 cells were resuspended in 10 mM $MgCl_2$ and .04% Silwet L-77 and diluted to $OD_{600} = .02$. The *A. thaliana* plants were sprayed from below and on top with inoculum. Discs of the infected leaves (one disc per leaf, .6 cm diameter) were excised at 1 dpi and 3 dpi. For one technical replicate, four leaf discs from one plant were pooled and ground in 200 µl 10 mM $MgCl_2$. Serial dilutions were plated on King's B medium with rifampicin (50 µg mL^{-1}) and bacterial colonies were quantified after two days of incubation at 28 °C. At least four plants per genotype and time points were harvested and plated. Results of three independent rounds of infection are included.

For qRT-PCR, for one technical replicate, two inoculated or mock-treated (sprayed with buffer-only) leaves per plant were harvested at 6 hpi, 1 dpi, and 3 dpi. Leaf material was ground using a tissue lyser and RNA extractions performed with Trizol reagent

(Invitrogen, USA) according to the manufacturer's protocol and the Zymo RNA Clean & Concentrator Kit, including in-column DNase treatment. RT-qPCR was performed using the NEB Luna® Universal One-Step RT-qPCR Kit (E3005) according to the manufacturer's instructions (55 °C 10 min, 95 °C 1 min, 95 °C 10 s, 60 °C 30 s, 45 cycles, and subsequent melting curve analysis). Reactions were set-up in duplicates using 10 ng RNA in 10 µl reactions. At least four samples per time point and treatment were analyzed, two rounds of infection were included.

4.3.7 | *X. campestris* pv. *campestris*

Plants for *X. campestris* pv. *campestris* infection were grown on soil with 10 h light and 55% humidity for four to five weeks. *X. campestris* pv. campestris 8004 was routinely grown at 28 °C on NYG (Nutrient Yeast Glycerol Agar, Daniels et al., 1984) media with 1% agar. Inoculum was prepared freshly by scraping bacteria from plates and resuspended in 1x PBS for a final OD_{600} of .4. Four leaves per plant were inoculated by application of 5 µl drops of bacterial suspension onto the midvein of leaves prior to pricking with a .4 * 20 mm needle five times. Plants were covered in a plastic bag for the first two days to create optimal infection conditions with high humidity. Discs of the inoculated leaves (one disc per leaf, .6 cm diameter) were excised at 3 dpi and 5 dpi. For one technical replicate, two leaf discs of one plant were pooled and ground in 200 µl 10 mM $MgCl_2$. Serial dilutions were plated on King's B medium supplemented with rifampicin (50 µg mL^{-1}), and bacterial colonies were quantified at two days after incubation at 28 °C. Suspensions that resulted in no colonies were excluded from the analysis. At least four samples per genotype and time point were harvested and plated. Results of three independent rounds of infection are included.

For qRT-PCR, for one technical replicate, two inoculated or mock-treated leaves per plant were harvested at 1 dpi, 3 dpi, and 7 dpi. RNA extraction and qRT-PCR reactions were performed as described above for *Pto* DC3000.

4.3.8 | *X. fastidiosa* subsp. *fastidiosa*

Plants for *X. fastidiosa* subsp. *fastidiosa* infection were grown on soil with 10 h light and 55% humidity for four to five weeks. *X. fastidiosa* subsp. *fastidiosa* Temecula1 (ATCC 700964) was routinely grown at 28 °C on PD3 plates (Pierce's Disease 3, Davis, 1980) for approx. seven to ten days. The inoculum was prepared freshly by scraping bacteria from the plate and resuspending it in 1x PBS for a final OD_{600} of .5. Four leaves per plant were inoculated by application of 5 µl drops of bacterial suspension onto the midvein of leaves prior to pricking with a .4 * 20 mm needle 5 times. For one technical replicate, two petioles per plant were combined and harvested at 5 dpi and 3 weeks post-inoculation (wpi). RNA was extracted from two petioles of infected samples after disruption with a tissue lyser, using Trizol reagent (Invitrogen, USA) according to the manufacturer's protocol and Zymo RNA Clean & Concentrator Kit, including in-column DNase treatment. qRT- PCR was performed with 10 ng RNA using the NEB Luna® Universal One-Step RT-qPCR Kit (E3005), in 10 µl reactions according to manufacturer guidelines (55 °C 10 min, 95 °C 1 min, 95 °C 10 s, 60 °C 30 s, 45 cycles, and subsequent melting curve analysis) using primers for *Xf16S* and *CDKA* (see Table S3) to normalize for plant material. At least four samples per genotype and time points were analyzed. Results of two independent rounds of infections are included.

For qRT-PCR, for one technical replicate, two inoculated leaves or mock-treated leaves per plant were harvested at 1 dpi, 5 dpi, and 3 wpi. RNA extraction and qRT-PCR reactions were performed as described above for *Pto* DC3000.

4.4 | Statistical analysis

All data was analyzed using R (version 2023.06.0 + 421) and statistical analysis was performed using the stats-package (R: The R Project for Statistical Computing, n.d.). For infection data, mutant measurements were compared to respective measurements in Col-0. For RT-qPCR and qPCR data analysis, expression values were analyzed using the $2^{(-\Delta\Delta ct)}$ method (Livak & Schmittgen, 2001) and normalized against *CDKA* or *UBC21* (*S. indica*) as housekeeping genes and the average of respective mock samples. For *E. cruciferarum*, all time points were compared to T0. Significance was assessed by two-sided Welch's *t*-test ($\alpha = .05$, *p*-values * < .05, ** < .01, *** < .001, **** < .0001) using the stats-package in R. Heat maps were generated using geom_tile of the ggplot package in R depicting average of normalized colonization compared to Col-0 at selected time point or average of log2 foldchange of gene expression at early, mid or late time point. We considered tissue from independently inoculated plants as technical replicates, which were pooled in some instances. Independent biological replicates of the experiments were performed to confirm results at least twice.

4.5 | Use of public data

The heat map showing the differential expression of *DCL* and *AGO* genes (Figure S1) was generated using data from Bjornson et al., 2021 (Tables S1 and S2) with Python v3.11.4 (Van Rossum & Drake, 1995) and Seaborn v0.12.2 (Waskom, 2021).

4.6 | Accession numbers

Genes reported in this article can be found in the GenBank/RGAP databases under the following accession numbers: *AGO1 (AT1G48410), AGO2 (AT1G31280), AGO4 (AT2G27040), AGO10 (AT5G43810), DCL2 (AT3G03300), DCL3 (AT3G43920), and DCL4 (AT5G20320), CDKA (AT3G48750.1), UBC21 (AT5G25760).*

AUTHOR CONTRIBUTIONS

A.R., H.T., S.N., B.L., S.F., J.K., J.S., E.S., S.K., V.G., M.F., A.W., K.H.K., R.P., S.R. designed the methodology; A.R., H.T., S.N., B.L., S.F., T.A., J.P., E.S. performed research; A.R., H.T., S.N., B.L., S.F., V.G., P.B., K.B. analyzed data; A.G., J.K., V.G., A.W., K.H.K., R.P., S.R. conceived the project and supervised the research; A.R., H.T., S.N., S.R. wrote the manuscript with input from all authors.

ACKNOWLEDGMENTS

This work was enabled by grants within the research unit FOR5116 "exRNA" funded by the Deutsche Forschungsgemeinschaft (DFG). Individual grants of this research unit comprise DFG projects FE448/15-1 to M. F, GO 2037/8-1 to A. G, GO 2064/4-1 to V. G., KE 856/8-1 to J.K., KO 1208/32-1 to K.K., PA 861/22-1 to R. P, RO 3550/16-1 to S.R. and WE 5707/2-1 to A.W. S.N. was supported by a Dr. Ernst-Leopold Klipstein Foundation grant. We thank Elif Olkun for technical support. Open Access funding enabled and organized by Projekt DEAL.

CONFLICT OF INTEREST STATEMENT

The authors declare no conflict of interest.

PEER REVIEW

The peer review history forthis article is available in the Supporting Information for this article.

DATA AVAILABILITY STATEMENT

The data that support the findings of this study are available from the corresponding author upon reasonable request.

ORCID

Alessa Ruf https://orcid.org/0000-0003-0919-9717
Sabrine Nasfi https://orcid.org/0000-0001-5916-0824
Johannes Postma https://orcid.org/0009-0002-0565-4487
Patrick Blumenkamp https://orcid.org/0000-0002-7013-9601
Alexander Goesmann https://orcid.org/0000-0002-7086-2568
Julia Kehr https://orcid.org/0000-0003-3617-9981
Jens Steinbrenner https://orcid.org/0000-0003-1008-2268
Arne Weiberg https://orcid.org/0000-0003-4300-4864
Karl-Heinz Kogel https://orcid.org/0000-0003-1226-003X
Ralph Panstruga https://orcid.org/0000-0002-3756-8957
Silke Robatzek https://orcid.org/0000-0002-9788-322X

REFERENCES

Agorio, A., & Vera, P. (2007). ARGONAUTE4 is required for resistance to *Pseudomonas syringae* in Arabidopsis. *The Plant Cell*, *19*(11), 3778–3790. https://doi.org/10.1105/tpc.107.054494

Azevedo, J., Garcia, D., Pontier, D., Ohnesorge, S., Yu, A., Garcia, S., Braun, L., Bergdoll, M., Hakimi, M. A., Lagrange, T., & Voinnet, O. (2010). Argonaute quenching and global changes in Dicer homeostasis caused by a pathogen-encoded GW repeat protein. *Genes & Development*, *24*(9), 904–915. https://doi.org/10.1101/gad.1908710

Bartsch, M., Gobbato, E., Bednarek, P., Debey, S., Schultze, J. L., Bautor, J., & Parker, J. E. (2006). Salicylic acid–independent ENHANCED DISEASE SUSCEPTIBILITY1 signaling in Arabidopsis immunity and cell death is regulated by the monooxygenase FMO1 and the Nudix hydrolase NUDT7. *The Plant Cell*, *18*(4), 1038–1051. https://doi.org/10.1105/tpc.105.039982

Bemm, F., Becker, D., Larisch, C., Kreuzer, I., Escalante-Perez, M., Schulze, W. X., Ankenbrand, M., de Weyer, A.-L. V., Krol, E., Al-Rasheid, K. A., Mithöfer, A., Weber, A. P., Schultz, J., & Hedrich, R. (2016). Venus flytrap carnivorous lifestyle builds on herbivore defense strategies. *Genome Research*, *26*(6), 812–825. https://doi.org/10.1101/gr.202200.115

Bjornson, M., Pimprikar, P., Nürnberger, T., & Zipfel, C. (2021). The transcriptional landscape of *Arabidopsis thaliana* pattern-triggered immunity. *Nature Plants*, *7*(5), 579–586. https://doi.org/10.1038/s41477-021-00874-5

Bouché, N., Lauressergues, D., Gasciolli, V., & Vaucheret, H. (2006). An antagonistic function for Arabidopsis DCL2 in development and a new function for DCL4 in generating viral siRNAs. *The EMBO Journal*, *25*(14), 3347–3356. https://doi.org/10.1038/sj.emboj.7601217

Bourras, S., Praz, C. R., Spanu, P. D., & Keller, B. (2018). Cereal powdery mildew effectors: A complex toolbox for an obligate pathogen. *Current Opinion in Microbiology*, *46*, 26–33. https://doi.org/10.1016/j.mib.2018.01.018

Cai, Q., Qiao, L., Wang, M., He, B., Lin, F.-M., Palmquist, J., Huang, S.-D., & Jin, H. (2018). Plants send small RNAs in extracellular vesicles to fungal pathogen to silence virulence genes. *Science*, *360*(6393), 1126–1129. https://doi.org/10.1126/science.aar4142

Cao, J.-Y., Xu, Y.-P., & Cai, X.-Z. (2020). Integrated miRNAome and transcriptome analysis reveals Argonaute 2-mediated defense responses against the devastating Phytopathogen *Sclerotinia sclerotiorum*. *Frontiers in Plant Science*, *11*, 500. https://doi.org/10.3389/fpls.2020.00500

Chen, D.-H., & Ronald, P. C. (1999). A rapid DNA minipreparation method suitable for AFLP and other PCR applications. *Plant Molecular Biology Reporter*, *17*(1), 53–57. https://doi.org/10.1023/a:1007585532036

Cheng, A.-P., Lederer, B., Oberkofler, L., Huang, L., Johnson, N. R., Platten, F., Dunker, F., Tisserant, C., & Weiberg, A. (2023). A fungal RNA-dependent RNA polymerase is a novel player in plant infection and cross-kingdom RNA interference. *PLOS Pathogens*, *19*(12), e1011885. https://doi.org/10.1371/journal.ppat.1011885

Consonni, C., Humphry, M. E., Hartmann, H. A., Livaja, M., Durner, J., Westphal, L., Vogel, J., Lipka, V., Kemmerling, B., Schulze-Lefert, P., Somerville, S. C., & Panstruga, R. (2006). Conserved requirement for a plant host cell protein in powdery mildew pathogenesis. *Nature Genetics*, *38*(6), 716–720. https://doi.org/10.1038/ng1806

Curaba, J., & Chen, X. (2008). Biochemical activities of Arabidopsis RNA-dependent RNA polymerase 6 *. *Journal of Biological Chemistry*, *283*(6), 3059–3066. https://doi.org/10.1074/jbc.M708983200

Daniels, M. J., Barber, C. E., Turner, P. C., Cleary, W. G., & Sawczyc, M. K. (1984). Isolation of mutants of *Xanthomonas campestris* pv. Campestris showing altered pathogenicity. *Microbiology*, *130*(9), 2447–2455. https://doi.org/10.1099/00221287-130-9-2447

Davis, M. J. (1980). Isolation media for the Pierce's disease bacterium. *Phytopathology*, *70*(5), 425. https://doi.org/10.1094/Phyto-70-425

Deleris, A., Gallego-Bartolome, J., Bao, J., Kasschau, K. D., Carrington, J. C., & Voinnet, O. (2006). Hierarchical action and inhibition of plant Dicer-like proteins in antiviral defense. *Science*, *313*(5783), 68–71. https://doi.org/10.1126/science.1128214

Dunker, F., Trutzenberg, A., Rothenpieler, J. S., Kuhn, S., Pröls, R., Schreiber, T., Tissier, A., Kemen, A., Kemen, E., Hückelhoven, R., & Weiberg, A. (2020). Oomycete small RNAs bind to the plant RNA-induced silencing complex for virulence. *eLife*, *9*, e56096. https://doi.org/10.7554/eLife.56096

Ellendorff, U., Fradin, E. F., de Jonge, R., & Thomma, B. P. H. J. (2009). RNA silencing is required for Arabidopsis defence against Verticillium

wilt disease. *Journal of Experimental Botany*, *60*(2), 591–602. https://doi.org/10.1093/jxb/ern306

Fang, X., & Qi, Y. (2016). RNAi in plants: An Argonaute-centered view. *The Plant Cell*, *28*(2), 272–285. https://doi.org/10.1105/tpc.15.00920

Frantzeskakis, L., Courville, K. J., Plücker, L., Kellner, R., Kruse, J., Brachmann, A., Feldbrügge, M., & Göhre, V. (2017). The plant-dependent life cycle of *Thecaphora thlaspeos*: A smut fungus adapted to Brassicaceae. *Molecular Plant-Microbe Interactions*, *30*(4), 271–282. https://doi.org/10.1094/MPMI-08-16-0164-R

Geng, S., Kong, X., Song, G., Jia, M., Guan, J., Wang, F., Qin, Z., Wu, L., Lan, X., Li, A., & Mao, L. (2019). DNA methylation dynamics during the interaction of wheat progenitor *Aegilops tauschii* with the obligate biotrophic fungus *Blumeria graminis* f Sp. *tritici*. *New Phytologist*, *221*(2), 1023–1035. https://doi.org/10.1111/nph.15432

Guo, N., Zhao, J., Yan, Q., Huang, J., Ma, H., Rajput, N. A., Jiang, H., Xing, H., & Dou, D. (2018). Resistance to *Phytophthora* pathogens is dependent on gene silencing pathways in plants. *Journal of Phytopathology*, *166*(6), 379–385. https://doi.org/10.1111/jph.12695

Hou, Y., Zhai, Y., Feng, L., Karimi, H. Z., Rutter, B. D., Zeng, L., Choi, D. S., Zhang, B., Gu, W., Chen, X., Ye, W., Innes, R. W., Zhai, J., & Ma, W. (2019). A *Phytophthora* effector suppresses trans-kingdom RNAi to promote disease susceptibility. *Cell Host & Microbe*, *25*(1), 153–165. e5. https://doi.org/10.1016/j.chom.2018.11.007

Huang, C.-Y., Wang, H., Hu, P., Hamby, R., & Jin, H. (2019). Small RNAs – Big players in plant-microbe interactions. *Cell Host & Microbe*, *26*(2), 173–182. https://doi.org/10.1016/j.chom.2019.07.021

Iwakawa, H.-O., & Tomari, Y. (2022). Life of RISC: Formation, action, and degradation of RNA-induced silencing complex. *Molecular Cell*, *82*(1), 30–43. https://doi.org/10.1016/j.molcel.2021.11.026

Ji, L., Liu, X., Yan, J., Wang, W., Yumul, R. E., Kim, Y. J., Dinh, T. T., Liu, J., Cui, X., Zheng, B., Agarwal, M., Liu, C., Cao, X., Tang, G., & Chen, X. (2011). ARGONAUTE10 and ARGONAUTE1 regulate the termination of floral stem cells through two MicroRNAs in Arabidopsis. *PLoS Genetics*, *7*(3), e1001358. https://doi.org/10.1371/journal.pgen.1001358

Jones, J. D. G., Staskawicz, B. J., & Dangl, J. L. (2024). The plant immune system: From discovery to deployment. *Cell*, *187*(9), 2095–2116. https://doi.org/10.1016/j.cell.2024.03.045

Jullien, P. E., Schröder, J. A., Bonnet, D. M. V., Pumplin, N., & Voinnet, O. (2022). Asymmetric expression of Argonautes in reproductive tissues. *Plant Physiology*, *188*(1), 38–43. https://doi.org/10.1093/plphys/kiab474

Kusch, S., Thiery, S., Reinstädler, A., Gruner, K., Zienkiewicz, K., Feussner, I., & Panstruga, R. (2019). Arabidopsis mlo3 mutant plants exhibit spontaneous callose deposition and signs of early leaf senescence. *Plant Molecular Biology*, *101*(1), 21–40. https://doi.org/10.1007/s11103-019-00877-z

Landa, B. B., Saponari, M., Feitosa-Junior, O. R., Giampetruzzi, A., Vieira, F. J. D., Mor, E., & Robatzek, S. (2022). Xylella fastidiosa's relationships: The bacterium, the host plants, and the plant microbiome. *New Phytologist*, *234*(5), 1598–1605. https://doi.org/10.1111/nph.18089

Li, Y., Zhang, Q., Zhang, J., Wu, L., Qi, Y., & Zhou, J.-M. (2010). Identification of MicroRNAs involved in pathogen-associated molecular pattern-triggered plant innate immunity. *Plant Physiology*, *152*(4), 2222–2231. https://doi.org/10.1104/pp.109.151803

Lincoln, C., Britton, J. H., & Estelle, M. (1990). Growth and development of the axr1 mutants of Arabidopsis. *The Plant Cell*, *2*(11), 1071–1080.

Livak, K. J., & Schmittgen, T. D. (2001). Analysis of relative gene expression data using real-time quantitative PCR and the $2^{-\Delta\Delta CT}$ method. *Methods*, *25*(4), 402–408. https://doi.org/10.1006/meth.2001.1262

López, A., Ramírez, V., García-Andrade, J., Flors, V., & Vera, P. (2011). The RNA silencing enzyme RNA polymerase V is required for plant immunity. *PLoS Genetics*, *7*(12), e1002434. https://doi.org/10.1371/journal.pgen.1002434

Martín-Merchán, A., Moro, B., Bouet, A., & Bologna, N. G. (2023). Domain organization, expression, subcellular localization, and biological roles of ARGONAUTE proteins in Arabidopsis. *Journal of Experimental Botany*, *74*(7), 2374–2388. https://doi.org/10.1093/jxb/erad030

Melotto, M., Zhang, L., Oblessuc, P. R., & He, S. Y. (2017). Stomatal defense a decade later. *Plant Physiology*, *174*(2), 561–571. https://doi.org/10.1104/pp.16.01853

Mitre, L. K., Teixeira-Silva, N. S., Rybak, K., Magalhães, D. M., de Souza-Neto, R. R., Robatzek, S., Zipfel, C., & de Souza, A. A. (2021). The Arabidopsis immune receptor EFR increases resistance to the bacterial pathogens *Xanthomonas* and *Xylella* in transgenic sweet orange. *Plant Biotechnology Journal*, *19*(7), 1294–1296. https://doi.org/10.1111/pbi.13629

Navarro, L., Dunoyer, P., Jay, F., Arnold, B., Dharmasiri, N., Estelle, M., Voinnet, O., & Jones, J. D. G. (2006). A plant miRNA contributes to antibacterial resistance by repressing auxin signaling. *Science*, *312*(5772), 436–439. https://doi.org/10.1126/science.1126088

Obbard, D. J., Gordon, K. H. J., Buck, A. H., & Jiggins, F. M. (2008). The evolution of RNAi as a defence against viruses and transposable elements. *Philosophical Transactions of the Royal Society, B: Biological Sciences*, *364*(1513), 99–115. https://doi.org/10.1098/rstb.2008.0168

Papenfort, K., & Melamed, S. (2023). Small RNAs, large networks: Post-transcriptional regulons in gram-negative bacteria. *Annual Review of Microbiology*, *77*, 23–43. https://doi.org/10.1146/annurev-micro-041320-025836

Qin, S., Veloso, J., Baak, M., Boogmans, B., Bosman, T., Puccetti, G., Shi-Kunne, X., Smit, S., Grant-Downton, R., Leisen, T., Hahn, M., & van Kan, J. A. L. (2023). Molecular characterization reveals no functional evidence for naturally occurring cross-kingdom RNA interference in the early stages of *Botrytis cinerea*–tomato interaction. *Molecular Plant Pathology*, *24*(1), 3–15. https://doi.org/10.1111/mpp.13269

R: The R Project for Statistical Computing. (n.d.). Retrieved 21 June 2024, from https://www.r-project.org/

Rebolledo-Prudencio, O. G., Estrada-Rivera, M., Dautt-Castro, M., Arteaga-Vazquez, M. A., Arenas-Huertero, C., Rosendo-Vargas, M. M., Jin, H., & Casas-Flores, S. (2022). The small RNA-mediated gene silencing machinery is required in Arabidopsis for stimulation of growth, systemic disease resistance, and suppression of the nitrile-specifier gene NSP4 by Trichoderma atroviride. *The Plant Journal*, *109*(4), 873–890. https://doi.org/10.1111/tpj.15599

Ren, B., Wang, X., Duan, J., & Ma, J. (2019). Rhizobial tRNA-derived small RNAs are signal molecules regulating plant nodulation. *Science*, *365*, 919–922. https://doi.org/10.1126/science.aav8907

Ried, M. K., Banhara, A., Hwu, F.-Y., Binder, A., Gust, A. A., Höfle, C., Hückelhoven, R., Nürnberger, T., & Parniske, M. (2019). A set of Arabidopsis genes involved in the accommodation of the downy mildew pathogen *Hyaloperonospora arabidopsidis*. *PLoS Pathogens*, *15*(7), e1007747. https://doi.org/10.1371/journal.ppat.1007747

del Sánchez-Correa, M. S., Isidra-Arellano, M. C., Pozas-Rodríguez, E. A., del Rocio Reyero-Saavedra, M., Morales-Salazar, A., del Castillo, S. M. L.-C., Sanchez-Flores, A., Jiménez-Jacinto, V., Reyes, J. L., Formey, D., & Valdés-López, O. (2022). Argonaute5 and its associated small RNAs modulate the transcriptional response during the rhizobia-Phaseolus vulgaris symbiosis. *Frontiers in Plant Science*, *13*, 1034419. https://doi.org/10.3389/fpls.2022.1034419

Šečić, E., Kogel, K.-H., & Ladera-Carmona, M. J. (2021). Biotic stress-associated microRNA families in plants. *Journal of Plant Physiology*, *263*, 153451. https://doi.org/10.1016/j.jplph.2021.153451

Šečić, E., Zanini, S., Wibberg, D., Jelonek, L., Busche, T., Kalinowski, J., Nasfi, S., Thielmann, J., Imani, J., Steinbrenner, J., & Kogel, K.-H. (2021). A novel plant-fungal association reveals fundamental sRNA and gene expression reprogramming at the onset of symbiosis. *BMC Biology*, *19*(1), 171. https://doi.org/10.1186/s12915-021-01104-2

Shen, D., Suhrkamp, I., Wang, Y., Liu, S., Menkhaus, J., Verreet, J.-A., Fan, L., & Cai, D. (2014). Identification and characterization of microRNAs in oilseed rape (*Brassica napus*) responsive to infection with the pathogenic fungus *Verticillium longisporum* using brassica AA (*Brassica rapa*) and CC (*Brassica oleracea*) as reference genomes. *New Phytologist*, *204*(3), 577–594. https://doi.org/10.1111/nph.12934

Silvestri, A., Fiorilli, V., Miozzi, L., Accotto, G. P., Turina, M., & Lanfranco, L. (2019). In silico analysis of fungal small RNA accumulation reveals putative plant mRNA targets in the symbiosis between an arbuscular mycorrhizal fungus and its host plant. *BMC Genomics*, *20*(1), 169. https://doi.org/10.1186/s12864-019-5561-0

Tang, Y., Yan, X., Gu, C., & Yuan, X. (2022). Biogenesis, trafficking, and function of small RNAs in plants. *Frontiers in Plant Science*, *13*, 825477. https://doi.org/10.3389/fpls.2022.825477

Taochy, C., Gursanscky, N. R., Cao, J., Fletcher, S. J., Dressel, U., Mitter, N., Tucker, M. R., Koltunow, A. M. G., Bowman, J. L., Vaucheret, H., & Carroll, B. J. (2017). A genetic screen for impaired systemic RNAi highlights the crucial role of DICER-LIKE 2. *Plant Physiology*, *175*(3), 1424–1437. https://doi.org/10.1104/pp.17.01181

Valdés-López, O., Formey, D., Isidra-Arellano, M. C., del Rocio Reyero-Saavedra, M., Fernandez-Göbel, T. F., & del Socorro Sánchez-Correa, M. (2019). Argonaute proteins: Why are they so important for the legume–*Rhizobia* symbiosis? *Frontiers in Plant Science*, *10*, 1177. https://doi.org/10.3389/fpls.2019.01177

Van Rossum, G., & Drake, F. L. Jr. (1995). *Python reference manual*. Centrum voor Wiskunde en Informatica Amsterdam.

Wang, Z., Hardcastle, T. J., Pastor, A. C., Yip, W. H., Tang, S., & Baulcombe, D. C. (2018). A novel DCL2-dependent miRNA pathway in tomato affects susceptibility to RNA viruses. *Genes & Development*, *32*(17–18), 1155–1160. https://doi.org/10.1101/gad.313601.118

Wang, Y., Pruitt, R. N., Nürnberger, T., & Wang, Y. (2022). Evasion of plant immunity by microbial pathogens. *Nature Reviews Microbiology*, *20*(8), 449–464. https://doi.org/10.1038/s41579-022-00710-3

Waskom, M. L. (2021). seaborn: Statistical data visualization. *Journal of Open Source Software*, *6*(60), 3021. https://doi.org/10.21105/joss.03021

Weiberg, A., Wang, M., Lin, F.-M., Zhao, H., Zhang, Z., Kaloshian, I., Huang, H.-D., & Jin, H. (2013). Fungal small RNAs suppress plant immunity by hijacking host RNA interference pathways. *Science*, *342*(6154), 118–123. https://doi.org/10.1126/science.1239705

Wong-Bajracharya, J., Singan, V. R., Monti, R., Plett, K. L., Ng, V., Grigoriev, I. V., Martin, F. M., Anderson, I. C., & Plett, J. M. (2022). The ectomycorrhizal fungus *Pisolithus microcarpus* encodes a microRNA involved in cross-kingdom gene silencing during symbiosis. *Proceedings of the National Academy of Sciences*, *119*(3), e2103527119. https://doi.org/10.1073/pnas.2103527119

Wook, K., Eamans, A. L., & Waterhouse, P. M. (2011). RNA processing activities of the Arabidopsis Argonaute protein family. In P. Grabowski (Ed.), *RNA processing*. INTECH. https://doi.org/10.5772/22686

Yu, X., Hou, Y., Chen, W., Wang, S., Wang, P., & Qu, S. (2017). *Malus hupehensis* miR168 targets to ARGONAUTE1 and contributes to the resistance against *Botryosphaeria dothidea* infection by altering defense responses. *Plant and Cell Physiology*, *58*(9), 1541–1557. https://doi.org/10.1093/pcp/pcx080

Zeise, K., & Von Tiedemann, A. (2002). Host specialization among vegetative compatibility groups of *Verticillium dahliae* in relation to *Verticillium longisporum*. *Journal of Phytopathology*, *150*(3), 112–119. https://doi.org/10.1046/j.1439-0434.2002.00730.x

Zhan, J., & Meyers, B. C. (2023). Plant small RNAs: Their biogenesis, regulatory roles, and functions. *Annual Review of Plant Biology*, *74*, 21–51. https://doi.org/10.1146/annurev-arplant-070122-035226

Zhang, X., Zhao, H., Gao, S., Wang, W.-C., Katiyar-Agarwal, S., Huang, H.-D., Raikhel, N., & Jin, H. (2011). Arabidopsis Argonaute 2 regulates innate immunity via miRNA393*–mediated silencing of a Golgi-localized SNARE gene, MEMB12. *Molecular Cell*, *42*(3), 356–366. https://doi.org/10.1016/j.molcel.2011.04.010

Zou, Y., Wang, S., Zhou, Y., Bai, J., Huang, G., Liu, X., Zhang, Y., Tang, D., & Lu, D. (2018). Transcriptional regulation of the immune receptor FLS2 controls the ontogeny of plant innate immunity. *The Plant Cell*, *30*(11), 2779–2794. https://doi.org/10.1105/tpc.18.00297

SUPPORTING INFORMATION

Additional supporting information can be found online in the Supporting Information section at the end of this article.

How to cite this article: Ruf, A., Thieron, H., Nasfi, S., Lederer, B., Fricke, S., Adeshara, T., Postma, J., Blumenkamp, P., Kwon, S., Brinkrolf, K., Feldbrügge, M., Goesmann, A., Kehr, J., Steinbrenner, J., Šečić, E., Göhre, V., Weiberg, A., Kogel, K.-H., Panstruga, R., Robatzek, S., & on behalf of the exRNA consortium (2024). Broad-scale phenotyping in Arabidopsis reveals varied involvement of RNA interference across diverse plant-microbe interactions. *Plant Direct*, *8*(11), e70017. https://doi.org/10.1002/pld3.70017